

Corresponding author:

Dr. Hong-Jian Feng

Room 324, nineteenth Dormitory,

XueYuan Road No.37 ,HaiDian District,

Beijing University of Aeronautics and Astronautics,

Beijing 100083, People's Republic of China

Tel.: +86-10-82328462

Fax: +86-312-3620575

Email address: fenghongjian@ss.buaa.edu.cn

fenghongjian@126.com

First-principles prediction of coexistence of magnetism and ferroelectricity in rhombohedral $\text{Bi}_2\text{FeTiO}_6$

Hong-Jian Feng , Fa-Min Liu

*Department of Physics, School of Science, Beijing University of Aeronautics and
Astronautics, Beijing 100083, P. R. China*

Abstract

First principles calculations based on the density functional theory within the local spin density approximation plus U(LSDA+U)scheme, show rhombohedral $\text{Bi}_2\text{FeTiO}_6$ is a potential multiferroic in which the magnetism and ferroelectricity coexist . A ferromagnetic configuration with magnetic moment of $4 \mu_B$ per formula unit have been reported with respect to the minimum total energy. Spontaneous polarization of $27.3 \mu \text{ C/cm}^2$,caused mainly by the ferroelectric distortions of Ti, was evaluated using the berry phase approach in the modern theory of polarization. The Bi-6s stereochemical activity of lone-pair and the ‘d⁰-ness’ criterion in off-centring of Ti were coexisting in the predicted new system. In view of the oxidation state of Bi^{3+} , Fe^{2+} , Ti^{4+} , and O^{2-} from the orbital-resolved density of states of the Bi-6p, Fe-3d, Ti-3d , and O-2p states, the valence state of $\text{Bi}_2\text{FeTiO}_6$ in the rhombohedral phase was found to be $\text{Bi}_2^{3+}\text{Fe}^{2+}\text{Ti}^{4+}\text{O}_6$.

Key words: Multiferroics; Density functional theory; Density of states

PACS: 71.15.Mb, 71.20.-b

1 Introduction

Multiferroic materials have coupled magnetic, electric, and even structural order parameters that result in ferromagnetic, ferroelectric, and/or ferroelastic properties at same phase. The magnetization can be rotated or even reversed by the ferroelectric reversal, and vice versa. These materials have potential applications in information storage, the emerging field of spintronics, and sensors. Since 1960s various articles have systematically classified their properties and behaviors [1,2,3,4,5], and the theoretical study was also carried out on the magnetoelectric coupling effect [6,7]. BiFeO₃ was the rare one in nature, which possess both weak ferromagnetism and ferroelectric characteristics in single phase. Meanwhile, more experimental investigation have been performed on the magnetoelectric properties of it. BiFeO₃ has long been known to be ferroelectric with a Curie temperature of about 1103 K and antiferromagnetic (AFM) with a Néel temperature of 643 K. The Fe magnetic moments were coupled ferromagnetically in the (111) plane and antiferromagnetically in the adjacent plane along [111] crystalline direction, which is called the G-type AFM. The rhombohedral distorted perovskite structure with space group $R\bar{3}c$ permits a canting of AFM sublattice, resulting in a weak ferromagnetism. However, there is a spiral spin structure in which the antiferromagnetic axis rotates through the crystal with a long-wavelength period of 620 Å [8]. Therefore, the linear magnetoelectric coupling was destroyed with the cancellation of magnetization, due to this long spiral spin structure. Although this cancellation could be suppressed partly in thin film, the magnetization observed in the BiFeO₃ thin film was relatively smaller in terms of the excellent ferroelectric behavior.

This cancellation of magnetization might be inhibited by doping foreign magnetic transitional metal ions such as Cr, Mn, Co, and Ni in the B sites. BiCrO₃ was recently synthesized and reported to be a highly distorted perovskite with *C2* symmetry[9], which permit the occurrence of ferroelectricity. Unfortunately, antiferromagnetic ordering was reported with a residual magnetization of 0.02 μ_B , suggestive of weak ferromagnetism. Bi₂FeCrO₆ has been predicted theoretically to be ferrimagnetic (2 μ_B per formula unit) and ferroelectric ($\sim 80 \mu C/cm^2$). The predicted ground state structure is very similar to the *R3c* structure of BiFeO₃, except that the Fe³⁺ in the second (111) plane are replaced by the Cr³⁺, which lead to the space group *R3*.

It is known that the ferroelectricity in BiFeO₃ is caused by the long Bi-6s stereochemically active pair, which formed the one chemical mechanism for stabilizing the ferroelectricity. This mechanism was caused by the mixing between the $(ns)^2$ ground state and a low-lying $(ns)^1(np)^1$ excited state, which can only occur if the cation ionic site does not have inversion symmetry. The second mechanism leading to the polarization in ferroelectrics is the off-centre displacement of small cation in the common perovskite ferroelectrics such as BaTiO₃, which is attributed to the ligand-field hybridization of the transitional metal cations by its surrounding anions. This mechanism requires the ‘d⁰-ness’ criterion in the small transitional metal off-centring, hence precludes the coexistence of magnetism and ferroelectricity. Sometimes these two mechanisms occur in the same material, such as PbTiO₃.

Due to the theories mentioned above, the Ti-doping BiFeO₃ could maintain these two behaviors together in same phase and generate the coexistence of magnetism and ferroelectricity. The new modified material Bi₂FeTiO₆ with rhombohedral structure was expected to have excellent magnetic and ferro-

electric properties. As in $\text{Bi}_2\text{FeCrO}_6$, the Fe^{3+} in the second (111) plane are replaced by the Ti^{4+} , which lead to the space group $R\bar{3}$. Up to now, there is no theoretical prediction on this new system. In this paper we have systematically investigated the electronic properties, ferroelectric behaviors, and magnetic ordering of the new theoretically predicted $\text{Bi}_2\text{FeTiO}_6$, using first principles calculation based on the density functional theory.

The remainder of this article is structured as follows: In section II, we presented the computational details of our calculations. We provided the calculated results and discussions in section III. In section IV, the conclusion based on our calculation were given.

2 Computational details

2.1 Methodology

Calculations in this work have been done using the Quantum-ESPRESSO package[10], which is based on the density functional theory(DFT) and density functional perturbation theory(DFPT) using the plane-wave pseudopotential formalism. We used our self-interaction-corrected ultrasoft pseudopotential implementation with the Perdew Burke Ernzerhof (PBE) exchange correlation functional, as the common local density approximation fail to obtain a band gap in the transitional metal oxides. In our DFT computations, plane-wave basis set with kinetic energy cut-off of 40 Ry was employed, and it has shown that the results are well converged at this cutoff. Bi 5d, 6s, and 6p electrons, Fe 3s, 3p, and 3d electrons, Ti 3s, 3p, and 3d electrons, and O 2s and O 2p electrons have been treated as valence states. We used up to $6 \times 6 \times 6$

grids of special k points in total energy calculation. In the local spin density approximation plus U(LSDA+U) framework, the strong Coulomb repulsion is treated by adding a Hubbard-like term to the effective potential, leading to an improved description of the interaction in the transitional metal oxides. The Hubbard parameter U in the range 0 eV - 8 eV were used in the calculation of electronic structures. Results show that the U of 7 eV is enough to produce a better insulated solution, which is used in the following sections.

2.2 *Structure optimization*

The lattice parameters was evaluated with respect to the lowest total energy ,ranging from 5.409 to 5.549 Å. In this process the structure was constrained to be rhombohedral within $R3$ space group. The atomic positions were taken from the corresponding value of BiFeO₃ in Ref.[11] , as the Fe³⁺ in the second (111) plane are replaced by the Ti⁴⁺ . The calculated lattice constant value was plotted with respect to energy and fitted to the Murnaghan equation of states ,which give the bulk modulus[12]. The atomic positions were relaxed afterward by minimization of the Hellman-Feynman forces within a convergency threshold of 10^{-3} Ry/Bohr , using Broyden-Fletcher-Goldfarb-Shanno(BFGS) variable metric method, as cell shape and volume was fixed.

We doubled the size of the unit cell along one of the rhombohedral lattice vectors and compared the total energies for all possible collinear spin configurations. The ferromagnetic(FM) and antiferromagnetic(AFM) structure (with nearest neighbor Fe antiparallel to each other) were constructed within the resulting supercell up to 20 atoms. Calculated energy show that the AFM structure supercell possess a relatively high energy of 0.03 eV per unit cell in

comparison with the FM one. The FM ordering along z and x(y) direction were considered to find the stable FM configuration. Total energy per formula unit show the FM ordering along z gave the stable magnetic configuration. Hence, in the following computation we took the FM ordering along z as the stable state .

2.3 *Spontaneous polarization*

In the modern theory of polarization approach[13,14,15], the total polarization \mathbf{P} for given crystalline geometry can be calculated as the sum of ionic and electronic contributions. The ionic contribution is calculated by summing the product of the position of each ion in the unit cell with the nominal charge of its rigid core. The electronic contribution is determined by evaluating the phase of the product of overlaps between cell-periodic Bloch functions along a densely-sampled string of neighboring points in k-space.

3 Results and discussion

The optimization of volume was performed with lattice constant ranging from 5.409 to 5.549 Å, and the volume plotted versus energy was shown in Fig.1. The calculated value was fitted to the Murnaghan equation of states, permitting to evaluate the bulk modulus. The normal parabolic curve gave the optimal value of 5.506 Å, compared with the corresponding value of 5.459 Å for BiFeO₃[11]. We also reported the magnetic moment per formula unit versus volume so as to see the variation of it with respect to volume change, and the optimal volume give a magnetic moment of 3.99 μ_B per formula unit. Next,

the atomic positions were relaxed using the optimal lattice constant with cell shape and volume fixed. The relaxing Wyckoff positions, calculated lattice constant, rhombohedral angles, and unit cell volumes were all summarized in Table I. The internal structural parameters are very similar to those in BiFeO_3 , except that the O positions were deviated from the initial positions. This may partly reflect the fact that there was a change of hybridization in the new predicted $\text{Bi}_2\text{FeTiO}_6$.

For the simple system consisting of N atoms, transforming the total Hamiltonian into Wannier representation for the narrow band gap condition we get

$$H = \sum_{i,j} \sum_{\delta} T_{ij} C_{i\delta}^+ C_{j\delta} + \frac{1}{2} \sum_{i,j,l,m} \sum_{\delta,\delta'} \langle ij|v|lm \rangle C_{i\delta}^+ C_{j\delta'}^+ C_{m\delta'} C_{l\delta} \quad (1)$$

The second term that is the interaction part can be simplified with considering the short distance effect on one lattice or atom as:

$$\frac{1}{2} U \sum_i \sum_{\delta,\delta'} C_{i\delta}^+ C_{i\delta'}^+ C_{i\delta'} C_{i\delta} = \frac{1}{2} U \sum_i \sum_{\delta} n_{i\delta} n_{i\bar{\delta}} \quad (2)$$

$n_{i\delta}$ and $n_{i\bar{\delta}}$ is the operator of spin-up and spin-down number of particles.

Here U is

$$\langle ii|v|ii \rangle = e^2 \int \frac{a^*(\mathbf{r} - \mathbf{R}_i) a^*(\mathbf{r}' - \mathbf{R}_i) a(\mathbf{r} - \mathbf{R}_i) a(\mathbf{r}' - \mathbf{R}_i)}{|\mathbf{r} - \mathbf{r}'|} d\mathbf{r} d\mathbf{r}' \quad (3)$$

Hence, U is the Coulomb interactions between the electrons around the lattice or atom and take great effect on the metal-insulator transition. The electronic structures were calculated with U varying from 0 eV to 8 eV. The results show the U of 7 eV is able to give a better insulated solution, while the insulated characteristics have not been improved significantly after increasing

of U further. We used this value of U in the following sections. The total density of states(DOS) for $\text{Bi}_2\text{FeTiO}_6$ before and after applying U was shown in Fig.2. It can be seen the band gap was increased from 0.46 eV ($U=0$ eV) to 1.68 eV($U=7$ eV). The top valence bands caused by Ti was pushed to the conduction bands after employed the U of 7 eV.

In order to gain more insight into the role of ferroelectric distortions on electronic structure and bonding behavior in these new predicted $\text{Bi}_2\text{FeTiO}_6$. The calculated band structure of up-spin states was given in Fig.3. There are strong hybridization between Bi-6p and O-2p states in the top of the valence bands, and the Fe-3d states was pushed down in lower energy region compared with those in BiFeO_3 . The strong hybridization also reflect the fact that the activity of Bi-6s long pair also take place in this new $R3$ structure. The band at -10 eV are mainly originating from the Bi-6s electrons ,these two bands are relative broader in this new system. Ti-3d bands mainly positioned at the bottom of conduction bands and hybridized deeply with O-2p states in this region, and the Ti 3d also overlap slightly with O 2p under the Fermi energy.

To understand the change of hybridization of Ti-O and Fe-O after Ti doping , the calculated charge density in the energy window from E_F-6 eV to E_F covering the region ,where the Ti-O bonding states are located ,were shown in Fig.4 and Fig.5,respectively. From these two Figures, it is clear that Ti is bonding strongly with O ,while Fe-O bonding strength is reduced comparing with those in BiFeO_3 . Moreover the Ti-O bonding is along the direction in which the Ti-3d orbitals formed and slightly affected by the ligand-field. It means the Ti is bonding deeply with the nearest six Oxygen atoms. Therefore the Ti off-centring driving ferroelectric displacement still maintained in these new system. We are expecting this chemical mechanism for stabilizing the

distorted structure in ferroelectric oxides take effect in the new system.

The Ti tend to form the oxidation state of Ti^{4+} , which can be approved by the orbital-resolved DOS for Ti shown in Fig.6 consequently. It is found the d_{xy} , d_{yz} , d_{z^2} , d_{xz} , and $d_{x^2-y^2}$ orbitals, including the majority spins and minority spins, are all nearly unoccupied in the conduction bands, indicating the oxidation state of Ti^{4+} . These bands are hybridizing strongly with the O-2p electrons, leading to the stabilizing ferroelectric off-centring behavior. And this phenomenon can further confirm the occurrence of this chemical mechanism in this predicted new system. The d_{yz} , d_{xz} , and $d_{x^2-y^2}$ orbitals have rather little states broadened under the Fermi energy, which indicate the smaller deviation of oxidation state from Ti^{4+} . These bands also overlap with O-2p electrons to strengthen the hybridization.

In the new structure, Fe atom tend to form oxidation state of Fe^{2+} , which is lowered comparing with the Fe^{3+} in BiFeO_3 . We reported the orbital-resolved DOS for Fe in BiFeO_3 and $\text{Bi}_2\text{FeTiO}_6$ shown in Fig.7 and Fig.8 respectively, so as to observe the change of oxidation states. It can be seen in Fig. 7 that all the majority spin states are occupied while all the minority spin states are nearly unoccupied with fewer states lying at -3.5 eV, indicating the oxidation state of Fe^{3+} in BiFeO_3 . However, from orbital-resolved DOS of Fe in $\text{Bi}_2\text{FeTiO}_6$ shown in Fig.8, unlike the case in BiFeO_3 , the spin-down states in d_{xy} and d_{xz} orbitals are partly occupied, indicating the orientation of bonding in this circumstance. Meanwhile all the spin-up states are occupied as in BiFeO_3 . Based on the large amount of occupied spin-down states in d_{xy} orbitals and the relatively fewer occupied spin-down states in d_{xz} orbitals, we deduced the formal spin ($S=4/2$) of Fe^{2+} with d^6 configuration in $\text{Bi}_2\text{FeTiO}_6$. Although the Fe-3d states were narrowed and pushed close to the Fermi energy after doping

with Ti, the main states have not overlapped deeply with the O-2p electrons. Hence the Fe 3d-O 2p hybridization have not been strengthened consequently.

The Bi-6s stereochemically active long pair were participating in the ferroelectric distortions. The hybridization between Bi-6p electrons and O-2p electrons can be observed in the orbital-resolved DOS of Bi and O in $\text{Bi}_2\text{FeTiO}_6$ shown in Fig.9. We also reported the total DOS in Fig. 9 for comparison. It is clear that the Bi-6p states and O-2p states positioned at the same energy region and hybridized strongly as in BiFeO_3 . Moreover, the Bi 6p does not change much comparing with the states in BiFeO_3 , indicating the similar oxidation states in these two systems. In view of the oxidation states of Ti^{4+} , Fe^{2+} , and Bi^{3+} , the valence state in the *R3* $\text{Bi}_2\text{FeTiO}_6$ is $\text{Bi}_2^{3+}\text{Fe}^{2+}\text{Ti}^{4+}\text{O}_6$.

The spontaneous polarization was evaluated using the berry phase method based on modern theory of polarization. And Born effective charges(BECs) were estimated by computing the Cartesian components of the polarization with respect to the atomic displacements, ie.:

$$\Delta P_\alpha \cong \sum_{j\beta} \frac{\partial P_\alpha}{\partial \mu_{j\beta}} (\mu_{j\beta} - \mu_{0j\beta}) = \frac{e}{\Omega} \sum_{j\beta} Z_{j\alpha\beta}^* \Delta \mu_{j\beta} \quad (4)$$

where $\Delta \mu_{j\beta}$ is the displacement of ion j in Cartesian direction β , $Z_{j\alpha\beta}^*$ is its BECs tensor, and Ω is the unit cell volume. The \mathbf{P} is calculated from berry phase method by considering a specific structural pathway parameterized by the change in atomic displacement connecting a centrosymmetric reference structure and *R3*. The displacement along [111] direction was chosen smaller (2% lattice constant) enough to ensure the validity of the linear treatment in Eq.(4). The results were listed in table II.

The new predicted $\text{Bi}_2\text{FeTiO}_6$ was found to obtain a medium value of spontaneous polarization of $27.3 \mu\text{C}/\text{cm}^2$, comparing with the relative large value of $59.4 \mu\text{C}/\text{cm}^2$ in BiFeO_3 . This result was not so good as we expected in terms of the coexistence of these two chemical mechanisms of ferroelectric distortions in the same phase. This phenomenon might be partly explained by the anomalous large BEC of 5.82 for Ti, leading to the dominant role of Ti off-centring distortions in the new predicted system. The producing polarization was similar to the value in BaTiO_3 [16] in which the same driving mechanism applied. Moreover, the BEC of Bi and Fe were all decreased in the new system, indicating the decreasing ability of producing the ferroelectricity of Bi-6s long-pair. There might be interaction between these two chemical mechanisms for producing ferroelectricity, which need to be explored further. The predominant role of Ti off-centring ferroelectric displacement generated a smaller ferroelectricity than the Bi-6s long-pair in terms of a collapse of $32 \mu\text{C}/\text{cm}^2$ in $\text{Bi}_2\text{FeTiO}_6$ compared with that in BiFeO_3 . Fortunately, the adoption of Ti in the new system inhibited the cancelling of macroscopic weak magnetization, accompanying the oxidation state of Fe^{2+} with d^6 configuration (with magnetic moment of $4 \mu_B$ per formula unit). Consequently, the coexistence of ferromagnetism and ferroelectricity can be fulfilled in the new predicted $\text{Bi}_2\text{FeTiO}_6$.

4 Conclusion

The cancellation of magnetization caused by the spiral spin structure ordering in BiFeO_3 can be improved by doping foreign transitional metal ions. $\text{Bi}_2\text{FeTiO}_6$ was predicted to be a potential multiferroic in which a large fer-

romagnetism(with magnetic moment of $4 \mu_B$ per unit cell) and ferroelectricity coexisted. Berry phase calculation show a medium polarization of $27.3 \mu C/cm^2$ in Bi_2FeTiO_6 comparing with the value of $59.4 \mu C/cm^2$ in $BiFeO_3$, which was mainly caused by the Ti off-centre ferroelectric distortions, although the hybridization between Bi-6p states and O-2p states had taken place in this new predicted system , which was reduced after doping Ti ,accompanying a small deviation of BECs of Bi from the nominal one. From the orbital-resolved DOS of the elements in the system ,the oxidation state of Bi_2FeTiO_6 was found to be $Bi_2^{3+}Fe^{2+}Ti^{4+}O_6$ with decreasing of oxidation state of Fe from Fe^{3+} to Fe^{2+} .

This work was supported by the Aeronautical Science foundation of China (Grant Nos. 2003ZG51069).

References

- [1] M. L. Plumer, M. B. Walker, J.Phys.C:Solid State Phys. 15 (1982) 7181.
- [2] V.J.Folen, G.T.Rado, E.W.Stalder, Phys.Rev.Lett. 6 (1961) 607.
- [3] R.B.Frankel, N.A.Blum, S.Foner, A.J.Freeman, M.Schieber, Phys.Rev.Lett. 15 (1965) 958.
- [4] R.Hornreich, S.Shtrikman, Phys.Rev. 161 (1967) 506.
- [5] L.M.Holmes, L. Uiter, Phys.Rev.B 5 (1972) 147.
- [6] H. YATOM, R. ENGLMAN, Phys.Rev. 188 (1969) 793.
- [7] R. ENGLMAN, H. YATOM, Phys.Rev 188 (1969) 803.
- [8] I. Sosnowska, T. Peterlin-Neumaier, E. Steichele, J.Phys.C:Solid State Phys. 15 (1982) 4835.

- [9] S.Niitaka, M.Azuma, M.Takano, E.Nishibori, M. Takata, M.Sakata, Solid State Ionics 172 (2004) 557.
- [10] S.Baroni, A. Corso, S. Gironcoli, P. Giannozzi, C.Cavazzoni, G. Ballabio, S.Scandolo, G. Chiarotti, P.Focher, A. Pasquarello, K.Laasonen, A.Trave, R.Car, N.Marzari, A.Kokalj, <http://www.pwscf.org/>.
- [11] J.Wang, J.b.Neaton, H. zheng, V.Nagarajan, S.B.Ogale, B.Liu, D.Viehland, V.Vaithyanathan, D.G.Schlom, U. Waghmare, N.A.spaldin, K.M.Rabe, M.Wuttig, R.Ramesh, Science 299 (2003) 1719.
- [12] F.D.Murnaghan, Pro.Natl.Acad.Sci.U.S.A 30 (1944) 244.
- [13] R.D.King-Smith, D.Vanderbilt, Phys.Rev.B 47 (1993) 1651.
- [14] D.Vanderbilt, R.D.King-Smith, Pyhs.Rev.B 48 (1994) 4442.
- [15] R.Resta, Rev.Mod.Phys 66 (1994) 899.
- [16] C.-G. Duan, S. S. Jaswal, E. Y. Tsymbal, Phys. Rev. Lett. 97 (2006) 047201.

Table 1

Calculated lattice constant a , rhombohedral angle α , volume V , and Wyckoff parameters for $\text{Bi}_2\text{FeTiO}_6$. The Wyckoff positions $1a(x,x,x)$ for the cations and $3b(x,y,z)$ for the anions.

		$\text{Bi}_2\text{FeTiO}_6$	BiFeO_3
$a(\text{\AA})$		5.506	5.459
$\alpha(^{\circ})$		60.36	60.36
$V(\text{\AA}^3)$		118.97	115.98
Bi	x	-0.001/0.501	0.000
Fe/Ti	x	0.229(Fe)/0.728(Ti)	0.231
O	x	0.558	0.542
	y	0.935	0.943
	z	0.393	0.398

Table 2

The polarization(P) and Born effective charges(BECs)(Z^*) for displacements along $[111]$ for $\text{Bi}_2\text{FeTiO}_6$ and BiFeO_3 .

	BiFeO ₃			Bi ₂ FeTiO ₆			
P(μ C/cm ²)	59.4			27.3			
	Bi	Fe	O	Bi	Fe	Ti	O
Z*	4.41	3.32	-2.58	3.61	1.89	5.82	-2.49

Figure captions:

Fig.1 Volume vs. total energy per formula unit and magnetic moment per formula unit for $\text{Bi}_2\text{FeTiO}_6$.

Fig.2 (a) and (b) show total DOS for $\text{Bi}_2\text{FeTiO}_6$ with $U=0$ eV and $U=7$ eV respectively. The Fermi level was set to zero.

Fig.3 Electronic band dispersion for $\text{Bi}_2\text{FeTiO}_6$. The Fermi level was set to zero.

Fig. 4 Charge density (in arbitrary units) in a particular plane for BiFeO_3 . The charge density is calculated in the energy window from E_F-6 eV to E_F .

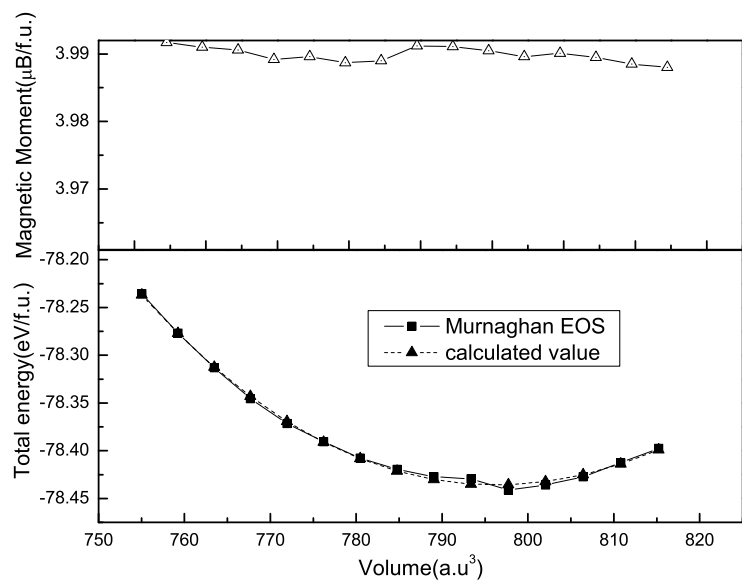
Fig. 5 Charge density (in arbitrary units) in a particular plane for $\text{Bi}_2\text{FeTiO}_6$. The charge density is calculated in the energy window from E_F-6 eV to E_F .

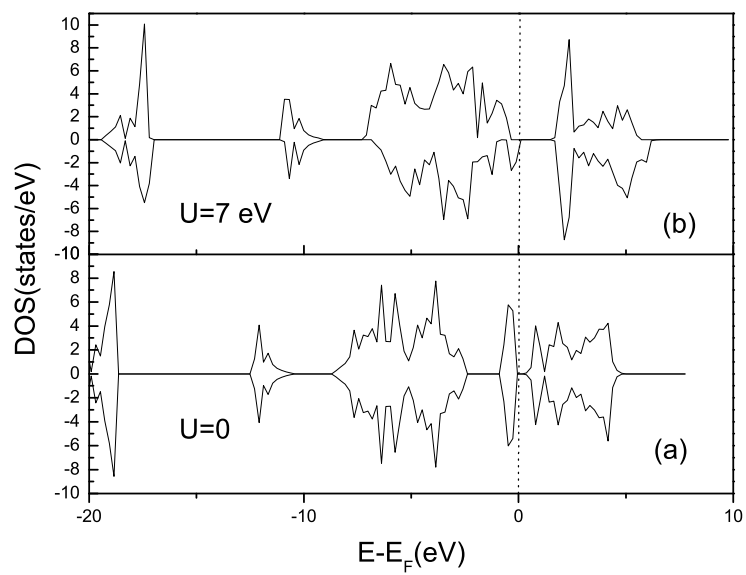
Fig. 6 Orbital-resolved DOS for Ti in $\text{Bi}_2\text{FeTiO}_6$. (a),(b),(c),(d),and (e) show the DOS for d_{xy} , d_{yz} , d_{z^2} , d_{xz} , and $d_{x^2-y^2}$ orbitals respectively. Spin-up states are shown in the upper portions and spin-down states in the lower portions in all panels. The Fermi level was set to zero.

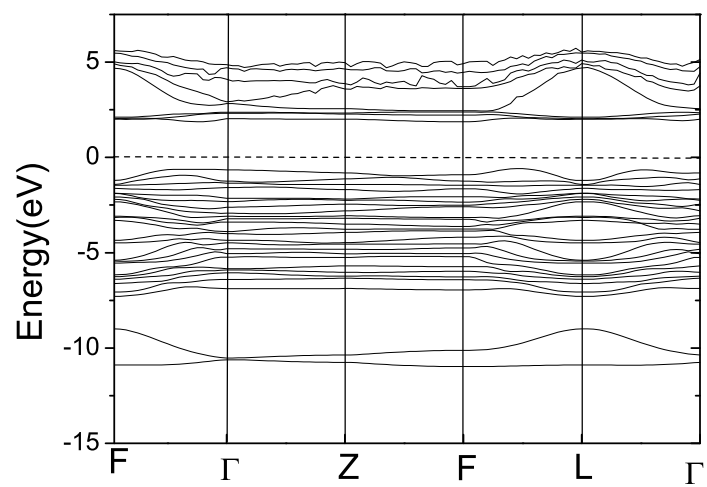
Fig. 7 Orbital-resolved DOS for Fe in BiFeO_3 . (a),(b),(c),(d),and (e) show the DOS for d_{xy} , d_{yz} , d_{z^2} , d_{xz} , and $d_{x^2-y^2}$ orbitals respectively. (f) show the Fe 3d total DOS. Spin-up states are shown in the upper portions and spin-down states in the lower portions in all panels. The Fermi level was set to zero.

Fig. 8 Orbital-resolved DOS for Fe in $\text{Bi}_2\text{FeTiO}_6$. (a),(b),(c),(d),and (e) show the d_{xy} , d_{yz} , d_{z^2} , d_{xz} , and $d_{x^2-y^2}$ orbitals respectively. Spin-up states are shown in the upper portions and spin-down states in the lower portions in all panels. The Fermi level was set to zero.

Fig. 9 Total DOS and orbital-resolved DOS for Bi 6p and O 2p in $\text{Bi}_2\text{FeTiO}_6$. (a) and (b) show the Bi-6p and O-2s states respectively. (c) is the total DOS. Spin-up states are shown in the upper portions and spin-down states in the lower portions in (c). The Fermi level was set to zero.







This figure "Figure4.jpg" is available in "jpg" format from:

<http://arXiv.org/ps/0710.2391v1>

This figure "Figure5.jpg" is available in "jpg" format from:

<http://arXiv.org/ps/0710.2391v1>

